




Geophysical Research Letters®



RESEARCH LETTER

10.1029/2022GL098857

Arrival of New Great Salinity Anomaly Weakens Convection in the Irminger Sea

T. C. Biló¹ , F. Straneo¹ , J. Holte¹ , and I. A.-A. Le Bras² 

¹Scripps Institution of Oceanography, University of California San Diego, La Jolla, CA, USA, ²Department of Physical Oceanography, Woods Hole Oceanographic Institution, Woods Hole, MA, USA

Key Points:

- Fresh anomaly identified in the Iceland Basin exhibits characteristics of a Great Salinity Anomaly (GSA) as it spreads into the Irminger Sea
- Within the Irminger Sea, the GSA was rapidly advected by the boundary currents while slowly spreading to the basin center
- Extreme freshening played a significant role in suppressing deep convection in the Irminger Sea during the 2018–2019 and 2019–2020 winters

Supporting Information:

Supporting Information may be found in the online version of this article.

Correspondence to:

T. C. Biló,
tcarrilhobilo@ucsd.edu

Citation:

Biló, T. C., Straneo, F., Holte, J., & Le Bras, I. A.-A. (2022). Arrival of new Great Salinity Anomaly weakens convection in the Irminger Sea. *Geophysical Research Letters*, 49, e2022GL098857. <https://doi.org/10.1029/2022GL098857>

Received 28 MAR 2022

Accepted 1 JUN 2022

Abstract The Subpolar North Atlantic is prone to recurrent extreme freshening events called Great Salinity Anomalies (GSAs). Here, we combine hydrographic ocean analyses and moored observations to document the arrival, spreading, and impacts of the most recent GSA in the Irminger Sea. This GSA is associated with a rapid freshening of the upper Irminger Sea between 2015 and 2020, culminating in annually averaged salinities as low as the freshest years of the 1990s and possibly since 1960. Upon the GSA propagation into the Irminger Sea over the Reykjanes Ridge, the boundary currents rapidly advected its signal around the basin within months while fresher waters slowly spread and accumulated into the interior. The anomalies in the interior freshened waters produced by deep convection during the 2017–2018 winter and actively contributed to the suppression of deep convection in the following two winters.

Plain Language Summary The Subpolar North Atlantic is prone to recurrent extreme freshening events (i.e., when the salinity decreases abruptly) called Great Salinity Anomalies (GSAs). As the circulation spreads them around the subpolar region, they indirectly contribute to the reduction of deepwater formation and weakening of the vertical transport of heat and anthropogenic carbon dioxide in the ocean. Here, we combine historical and new moored temperature and salinity records to document the arrival, spreading, and impacts of the most recent GSA in the Irminger Sea. This GSA led to a rapid freshening of the Irminger Sea between 2015 and 2020, 2–4 times faster than the freshening rates registered in the previous 10 years. This event culminated in annually averaged salinities as low as the freshest years of the 1990s and possibly since 1960. Tracking the GSA's path in the subpolar gyre, we found that the GSA flows with the boundary currents along the basin's rim within months while other processes slowly spread the fresher waters to the central Irminger Sea. The accumulation of fresher waters in the basin's center freshened the deep water formed during the 2017–2018 winter and actively contributed to the halt of deepwater formation in the following two winters.

1. Introduction

The Atlantic Meridional Overturning Circulation (AMOC) is an essential regulator of the Earth's climate. In the Subpolar North Atlantic (SPNA, 45°–65°N), the warm and salty waters of the AMOC's upper limb are subject to significant heat loss to the atmosphere (Lozier, 2010). This cooling drives surface water mass transformation, contributing to the overturning (Lozier, 2012) and the vertical transport of heat and anthropogenic carbon dioxide in the ocean (e.g., Fröb et al., 2016). Therefore, changes in the rate of water mass transformation associated with the SPNA's hydrographic variability have the potential to impact the AMOC and consequently the global climate system.

One important component of the AMOC is the winter convective activity in the Irminger Sea (~30°–45°W). In this region, wintertime convection forms Irminger Sea Intermediate Water (ISIW), which, together with Labrador Sea Water (LSW), constitutes the upper portion of the AMOC's lower limb known as the upper-North Atlantic Deep Water (Le Bras et al., 2020; Pickart et al., 2003). Specifically, deep convection—that is, atmospheric-forced water mass transformation from the surface to depths greater than 700–1,000 m—forms deep ISIW within $27.73 < \sigma_0 < 27.77 \text{ kg m}^{-3}$ (Le Bras et al., 2020); is mostly constrained near the center of the basin and south of Greenland (Piron et al., 2016); and its occurrence and strength are sensitive to favorable atmospheric and ocean stratification conditions (de Jong et al., 2012, 2018; Vage et al., 2009). Upper ocean stratification in the SPNA, in turn, is strongly affected by the surface salinity variability (e.g., Våge et al., 2011). Between 1960 and 2000, extreme surface freshening events, known as Great Salinity Anomalies (GSAs), have impacted the SPNA every ~10–15 years (Belkin, 2004). These salinity anomalies, which originate from anomalous ice/freshwater fluxes

© 2022. The Authors.

This is an open access article under the terms of the [Creative Commons Attribution License](https://creativecommons.org/licenses/by/4.0/), which permits use, distribution and reproduction in any medium, provided the original work is properly cited.

from the Arctic Ocean to the SPNA, spread throughout the SPNA, weakening or even suppressing wintertime deep convection (e.g., Lazier, 1980). Recently, Holliday et al. (2020) documented an unprecedented basin-wide freshening event in the Iceland Basin ($\sim 20^{\circ}$ – 30° W) between 2012 and 2016. Combining an extensive collection of salinity observations and atmospheric reanalysis, the authors showed that anomalous atmospheric conditions diverted and redistributed, in 4 years, approximately $4,600 \text{ km}^3$ of freshwater away from Labrador's continental margin toward the interior of the Iceland Basin. As a result, the salinity of the upper 200 m decreased approximately 0.2 practical salinity units (PSU), which represents the strongest freshening of the last 120 years. Although the origin of this recent salinity anomaly is distinct from previously reported GSAs, its strength and freshwater content are comparable in magnitude to previous events. For example, in 5 years, $\sim 10,000 \text{ km}^3$ of freshwater entered the Nordic Seas and SPNA in the late 1960s (Curry & Mauritzen, 2005), causing the strongest salinity decrease (~ 0.4 PSU) ever recorded in the Labrador Sea (Dickson et al., 1988). This suggests that the recent event might be a new GSA of the SPNA.

In addition to the freshening discussed in Holliday et al. (2020), recent observational and numerical studies indicate that the total amount of salt and heat in the SPNA has significantly decreased between ~ 2010 and 2017. This decrease is attributed to the ocean's forced response to the atmospheric mode of variability known as the North Atlantic Oscillation (NAO; Lankhorst & Send, 2020; Tesdal & Haine, 2020). The NAO is highly correlated with the strength of the SPNA circulation (Häkkinen & Rhines, 2004) as well as the flux of warm and saline subtropical water masses into the SPNA (Hátún et al., 2005; Våge et al., 2011) on interannual-to-decadal time scales. Holliday et al. (2020) acknowledge that the decrease of subtropical water fluxes might have also contributed to this hypothesized "new GSA" formation, raising the question of the water mass composition of the freshened regions.

A common characteristic of previous GSAs is their advection by the SPNA's cyclonic circulation. Freshening of the upper waters in the Irminger Sea has been attributed to the cyclonic propagation of the 2012–2016 freshening event in the Iceland Basin from in situ observations (de Jong et al., 2020; Zunino et al., 2020). However, these observations do not cover the entire Irminger basin or last long enough to assess the development and propagation of the freshening signal, its impacts on ISIW formation, or its relative strength to GSAs in the area.

In the present study, we combine hydrographic ocean analyses and moored observations simultaneously collected at different locations across the SPNA to document the arrival, spreading, and impact on convection in the Irminger Sea of a new GSA between 2015 and 2020. We find that the spreading of the unprecedented anomaly from the Iceland Basin led to salinities in the Irminger Sea similar to salinities registered in the 1990s and, possibly, historic lows since the 1960s, contributing to the halt of deep convection and to the formation of significantly fresher and lighter ISIW.

2. Data and Methods

2.1. Hydrographic Ocean Analyses and Auxiliary Products

We mainly utilized two different hydrographic climatological objectively mapped products to investigate the basin-wide salinity interannual variability: (a) Roemmich–Gilson (RG) Argo floats monthly climatology (Roemmich & Gilson, 2009); (b) EN4 hydrographic monthly climatology (Good et al., 2013, version 4.2.1) with the Gouretski and Reseghetti (2010)'s bias correction. The RG-climatology (EN4) has global coverage of 1° horizontal resolution at 58 (42) different vertical levels from near the surface to approximately 2,000 m (5,350 m) between 2004 and 2021 (1900 and 2021). We complement our analysis by using individual quality-controlled Argo profiles (Argo, 2020), the ocean eddy-resolving reanalysis GLORYS12 (Jean-Michel et al., 2021), and the ARMOR3D hydrographic climatology (Guinehut et al., 2012) as auxiliary climatologies.

To quantify the recent salinity changes in the Irminger Sea, we estimated the 2015–2020 linear salinity trends using the RG-climatology. Next, by combining RG and EN4, we investigated the basin-wide average near-surface salinity changes for the period 1960–present. We used the auxiliary climatologies to assess the robustness of the signal (Text S1 in Supporting Information S1). The Irminger Sea is defined as the region bounded between the Reykjanes Ridge and Cape Farewell ($\sim 30^{\circ}$ – 45° W), and the parallels 58° – 65° N (Figures 1a and 1b). Finally, we tracked the salinity anomalies in the RG-climatology to investigate the GSA spreading pathways.

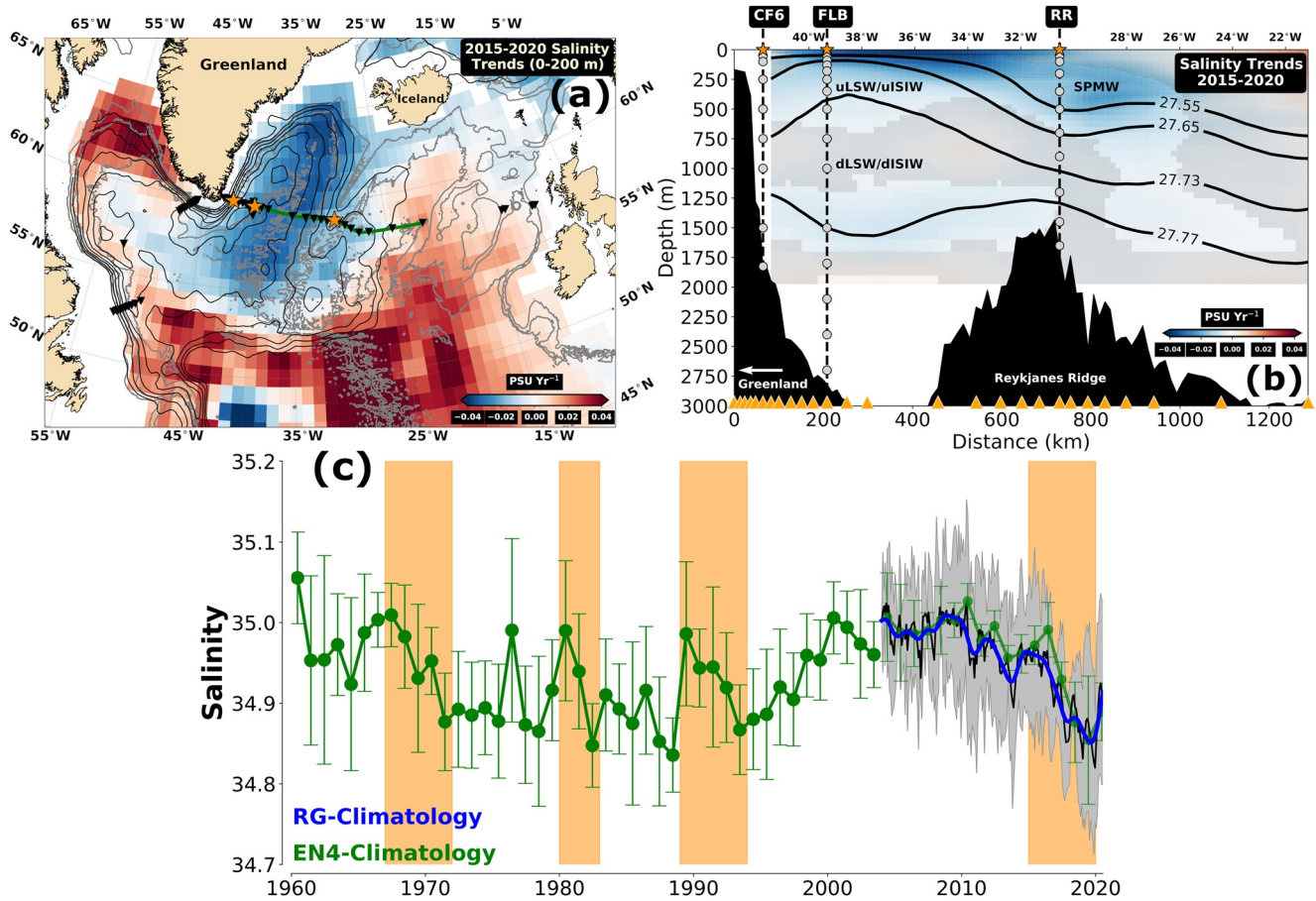


Figure 1. (a) 2015–2020 salinity trends averaged in the upper 200 m and (b) 2015–2020 salinity trends at the Overturning in the Subpolar North Atlantic Program (OSNAP) East array (i.e., solid green line in (a)) from the RG-climatology. The triangles indicate the OSNAP and Ocean Observatories Initiative (OOI) moorings locations in the Subpolar North Atlantic (SPNA), and the stars highlight the CF6, FLB, and RR moorings. Gray lines in (a) are the 1,000, 2,000, and 3,000 m isobaths, while black lines represent 2015–2020 mean absolute dynamic topography isolines (or geostrophic stream function) from AVISO equally spaced in 0.05 m between -0.65 and -0.35 m. Gray circles and solid lines in (b) are the pointwise CTD locations on the highlighted moorings, and the 2015–2020 mean potential density (σ_θ) surfaces in kg m^{-3} , respectively. Shaded areas show where the salinity trends are not statically significant at the 95% confidence level. (c) Annual and 18-month low-passed filtered time series of the average salinity within the Irminger Sea’s upper 200 m depth from EN4 (solid green line) and RG (solid blue line) climatologies, respectively. The thin black line is the RG-climatology monthly salinity values. Uncertainties represent the 95% confidence interval of the EN4 annual averages (green dots) and the Argo monthly averages (shaded gray areas). Finally, orange highlighted periods show the 1960s–1970s, 1980s, 1990s, and the most recent (i.e., 2015–2020) hypothesized Great Salinity Anomalies in the SPNA. Salinity units are practical salinity units. Acronyms and abbreviations: RR, Reykjanes Ridge; uLSW, upper Labrador Sea Water; dLSW, deep Labrador Sea Water; uISIW, upper Irminger Sea Intermediate Water; dISIW, deep Irminger Sea Intermediate Water; SPMW, Subpolar Mode Water.

We also used the 30-arc second resolution gridded topography from GEBCO, surface drifters trajectories from the Global Drifters Program between 1990 and 2020 (Elipot et al., 2016), and the daily $1/4^\circ$ resolution absolute dynamic topography product from Ssalto/Duacs distributed by Aviso+ to aid in the interpretation of the results. The latter is part of the CNES/SALP project with the support of the Copernicus Marine Environment and Monitoring Service, and we refer to it as the SPNA barotropic geostrophic stream function.

2.2. Mooring Arrays

Although the hydrographic monthly climatologies can provide an overview of the interannual salinity changes in the study region, the Argo array is limited to areas seaward of the 1,000–2,000 m isobaths, only partially resolving the boundary current systems (Biló & Johns, 2019; Holte & Straneo, 2017). Therefore, it is reasonable to assume that the objectively mapped RG-climatology is poorly constrained by in situ Argo data near the western boundary and over the Reykjanes Ridge. To describe water properties near boundaries, where Argo is uncertain or unavailable, we analyzed moored hydrographic observations.

These observations are from the Overturning in the Subpolar North Atlantic Program (OSNAP, Lozier et al., 2019) and Ocean Observatories Initiative (OOI, e.g., de Jong et al., 2018) mooring arrays within the Irminger Sea (Figures 1a and 1b). In the present study, we focused our analysis on the mooring OSNAP-RR at the eastern side of the basin (aka M1, Koman et al., 2020), OSNAP-CF6 within the western boundary (Le Bras et al., 2018), and the OOI-FLB in the central Irminger Sea (Hopkins et al., 2019). All moorings include stationary CTD instruments, which measured salinity, temperature, and pressure every 15 min to 1 hr between August 2014 and July 2020. These instruments are typically separated by tens of meters in the upper 300 m and by a few hundreds of meters in the deep ocean (Figure 1b). Details of the processing and quality control of the data are contained (Text S2 in Supporting Information S1).

2.3. Buoyancy Content, Surface Buoyancy Fluxes, and Signal Processing

We evaluated the interannual salinity variability impact on the convective activity of the Irminger Sea by calculating the water column buoyancy content (B) using the moored observations and by estimating the local atmospheric buoyancy forcing fluxes (B_{flux}) from the European Centre for Medium-Range Weather Forecasts ERA5 reanalysis (Dee et al., 2011). Following Schmidt and Send (2007), we defined B as

$$B = \frac{g}{\rho_0} \int_0^z (\sigma_{0z} - \sigma_0) dz, \quad (1)$$

where z is the vertical coordinate pointing toward the ocean bottom, $g = 9.8 \text{ m s}^{-2}$ the acceleration due to gravity, $\rho_0 = 1,027 \text{ kg m}^{-3}$ a reference density, and σ_0 (σ_{0z}) is potential density at the surface (depth = z). We estimated B_{flux} as the sum of the equivalent buoyancy flux due to surface heat fluxes and surface freshwater fluxes (Equation 2, Gill, 1982):

$$B_{flux} = \frac{g\alpha}{\rho_0 C_p} Q_{net} - \beta g S_0 (E - P), \quad (2)$$

where α is the seawater thermal expansion coefficient, C_p the seawater heat capacity, Q_{net} is the surface net heat flux, β haline expansion coefficient, S_0 sea surface salinity, E evaporation rate, and P precipitation rate. The parameters α , β , and C_p are calculated based on the temperature and salinity measurements of the uppermost instruments in each mooring (i.e., ~ 30 – 50 m depth). We estimated all parameters and potential density using the Gibbs Seawater Oceanographic Toolbox 3.05 software (McDougall & Barker, 2011).

We isolated the interannual variability by low-pass filtering the moored and RG time series. Our filtering procedure consists of a fourth-order Butterworth filter (e.g., Emery & Thomson, 2001) with a cutoff period of 18 months which allowed us to observe the GSA's spreading and evolution (e.g., Sections 3.1 and 3.2). Unfortunately, due to nonrealistic monthly oscillations and the lack of data constraining the EN4 objective mapping before the Argo period, the EN4 monthly-to-annual salinity variability presents largely uncertain and nonrealistic amplitude and frequency characteristics within the study region (see Text S1 in Supporting Information S1 for details). Although the EN4 seems to fail to depict monthly-to-annual time scales, its interannual-to-decadal time scales are consistent with other climatological products. Since we limited our analysis of the EN4 to its salinity basin-wide interannual variability, we bypassed this issue by applying low-pass filters with cutoff periods longer than 2.5–3 years. However, important variability near the end of the time series was over smoothed, and filter edge effects were amplified (not shown). To avoid these problems, we opted to evaluate the EN4 interannual variability as annual averages.

3. Results and Discussion

3.1. The Rapid Basin-Wide Freshening of the Upper Irminger Sea

Between 2015 and 2020, the upper 200 m freshened (i.e., negative salinity trends) over the northern and western Iceland Basin, Irminger Sea, and the central Labrador Sea (Figure 1a). The strongest freshening occurred over the central areas of the Irminger Sea, varying from -0.02 to $-0.04 \text{ PSU year}^{-1}$. These trends were not confined to the ocean surface (Figure 1b), though they significantly decrease below 200 m and within isopycnal layers denser than $\sigma_0 = 27.65 \text{ kg m}^{-3}$. Nonnegligible negative trends (i.e., up to $-0.01 \text{ PSU year}^{-1}$) were also present in intermediate (i.e., 200–1,000 m) and deep ($z > 1,000$ m) regions of the Irminger Sea.

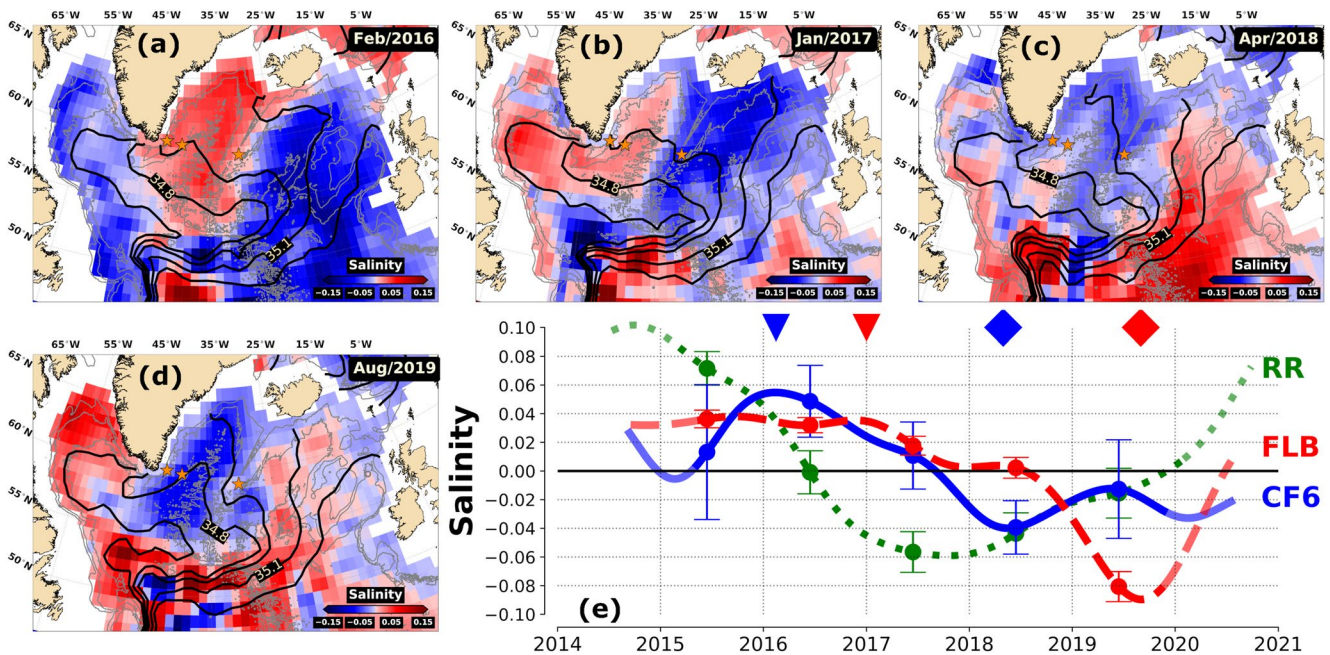


Figure 2. RG-climatology (a) February 2016, (b) January 2017, (c) April 2018, and (d) August 2019 18-month low-pass filtered salinity anomalies averaged between 0 and 200 m depth relative to the Overturning in the Subpolar North Atlantic Program (OSNAP) moorings data period. Black lines are the 34.7, 34.8, 34.9, 35.1, and 35.3 isohalines, while gray lines represent the 1,000, 2,000, and 3,000 m isobaths. Stars highlight the locations of CF6, FLB, and RR moorings. (e) Eighteen-month low-pass filtered salinity anomalies averaged between 0 and 200 m depth measured by the CF6 (western boundary), FLB (interior), and Reykjanes Ridge moorings. The transparent portion of the curves represents the periods under the low-pass filter edge effects. Error bars show the 95% confidence interval of annual salinity averages. The blue (red) triangles and diamonds represent the start and end of the freshening period in the CF6 (FLB) records, respectively. They also represent the times of the (a)–(d) maps. Salinity units are practical salinity units.

The Irminger Sea’s surface intensified freshening is associated with an average salinity decrease of approximately -0.11 (-0.15) PSU between January 2016 and August 2019 from the RG-climatology (EN4-climatology; Figure 1c). Note that this 2015–2020 freshening is much more pronounced than the weaker freshening that started around 2010. As a result of the combined effects of this weaker freshening (2010–2015) and the recent rapid event after 2015, 2019 corresponds to the freshest state of the Irminger Sea since the early 1990s (Figure 1c).

Sharp salinity decrease, however, is not unique to the 2015–2020 period. Similar rapid freshening episodes (i.e., 0.15–0.2 PSU drop) have occurred in the Irminger Sea consistent with the presence of GSAs in the SPNA reported in the literature: 1960s–1970s GSA (Dickson et al., 1988), 1980s GSA (Belkin et al., 1998), and 1990s GSA (Belkin, 2004; Figure 1c). Unfortunately, the limited data do not allow us to quantify the precise amplitudes of the anomalies before 2004 (see Section 2.3 and Text S1 in Supporting Information S1). However, based on annual averages, it is reasonable to conclude that the signal in 2016–2019 is among the fastest salinity decreases ever recorded in the study region (i.e., up to 0.04 PSU year⁻¹). The average salinity in 2019 was as low as the freshest years of the 1990s, and possibly, since 1960.

Not surprisingly, the unprecedented 2012–2016 freshening in the upper Iceland Basin was followed by a rapid basin-wide freshening of the Irminger Sea after 2015. This event corresponds to salinity trends approximately 2–4 times the trends registered in the previous decade (Tesdal et al., 2018), suggesting that the recent freshening identified by Holliday et al. (2020) indeed propagated from the Iceland Basin to the Irminger Sea. Finally, based on this event’s intensity, freshwater content, vast spatial extent, and advection by the SPNA’s circulation, it is reasonable to treat the recent freshening event as a new GSA of the SPNA.

3.2. Salinity Anomalies Spreading and Pathways

The GSA over the Iceland Basin propagated westward mainly over the Reykjanes Ridge, freshening the Irminger Sea after 2015 (see negative salinity, or fresh, anomalies in Figures 2a–2d). Once fresh anomalies propagated past southern Iceland and across the ridge in early 2016, they were rapidly advected by the boundary currents

around the Irminger Sea (Figure 2b), while slowly spreading to the central Irminger Sea until the freshening peak in August 2019 (Figures 2c and 2d).

Further analyzing the GSA's spreading patterns into the interior, we observe that different periods present specific spreading characteristics (see Movie S1). Between January 2017 and December 2018, fresh anomalies propagate away from the boundary current system. In contrast, the freshening during 2019 intensifies locally (i.e., quasi-stationary development). Anomalies propagation patterns in 2019 suggest that anomalies from the central Labrador and Iceland Basins enter the central Irminger through its southern boundary and tend to locally accumulate. We acknowledge that other processes contributing to this freshwater accumulation and freshening intensification might play a role in 2019 (e.g., increase in precipitation and surface wind-driven freshwater convergence), and further research is still required.

The GSA's arrival in the Irminger Sea is associated with significant interannual salinity decreases of approximately 0.16 ± 0.03 PSU over the Reykjanes Ridge (RR, December 2014 to October 2017), followed by $\sim 0.11 \pm 0.06$ PSU in the western boundary (CF6, February 2016 to April 2018), and $\sim 0.12 \pm 0.02$ PSU in the central Irminger (FLB, January 2017 to August 2019; Figure 2e). The interannual salinity variability explains approximately 44%, 13%, and 69% of the total variance of the RR, CF6, and FLB mooring records, respectively. Although the year-to-year variations do not account for the major portion of the western boundary variance as in the other locations, ~ 0.11 PSU salinity decrease is not negligible, approximately corresponding to the average seasonal cycle's amplitude (Figure S2 in Supporting Information S1).

Note that the freshening signal at the western boundary (central Irminger) peaks approximately 6 (22) months after peaking over the Reykjanes Ridge (Figure 2e). These qualitatively obtained transit times corroborate the Argo observations of the fresh anomalies' fast advection by the boundary current and their slow spreading to the interior. To properly quantify the GSA's spreading time scales, we perform a cross-correlation analysis of the mooring records and study surface drifters trajectories spreading (e.g., Miron et al., 2017). Both cross correlations (Figure S3 in Supporting Information S1) and drifters (Figure S4 in Supporting Information S1) suggest that fresh anomalies can take about 6–11 months to travel between the Reykjanes Ridge and east Greenland, which corresponds to advective spreading rates of 0.07 – 0.11 m s⁻¹ along the boundary current (i.e., $\sim 1,700$ km separate RR and CF6). Our advective speed estimates are in reasonably good agreement with measured velocities around the basin (de Jong et al., 2020; Vage et al., 2011). Finally, our cross-correlation analysis indicates that salinity anomalies over the ridge could take up to 21–29 months to impact the central Irminger (see Discussion in the Supporting Information for details).

To summarize, we showed that the main pathway of the recent GSA from the Iceland Basin to the Irminger Sea is over the Reykjanes Ridge. Over the ridge, the anomalies probably follow the narrow westward flows within the deeper ridge fractures (Koman et al., 2020; Petit et al., 2018, 2019) impacting the boundary current in the eastern Irminger Sea over the 2015–2017 period (e.g., de Jong et al., 2020). While the boundary current system can advect the GSA signal within months between the ridge and east Greenland, anomalies can take up to 2.5 years to spread from the ridge to the basin's center. As a result, the freshening within the western boundary starts roughly 1 year before and lasts 6 months less than the freshening in the central Irminger. Additionally, the timing and duration of the freshening at each location also explain why the 2015–2020 linear salinity trends (Figure 1) decrease toward the boundaries of the Irminger Sea. Our analysis does not allow us to infer the dynamical mechanisms responsible for this “boundary-to-interior slow spreading” of the salinity anomalies. However, hydrographic observations indicate that mesoscale eddies (Fan et al., 2013) and interior recirculation (Holliday et al., 2007, 2009) could control the exchange of waters between the boundary and the interior.

3.3. GSA Impacts on the Stratification and Convection

As mentioned in Section 1, the central Irminger Sea is a crucial area for the SPNA convective activity that contributes to the AMOC's lower limb. Therefore, the recent presence of a GSA over the upper Irminger Sea could significantly impact deep ISIW (dISIW) formation via convection. Here, we investigate the impact of this anomaly on the ocean stratification (i.e., buoyancy content) and convection activity using the temperature and salinity measurements from mooring FLB and the atmospheric conditions from the ERA5 reanalysis.

Figure 3a shows the moored TS profiles in the central Irminger prior to (i.e., late fall) and at the end of (i.e., late winter) the deep convection season for each year. The temporal evolution of the fall profiles clearly shows

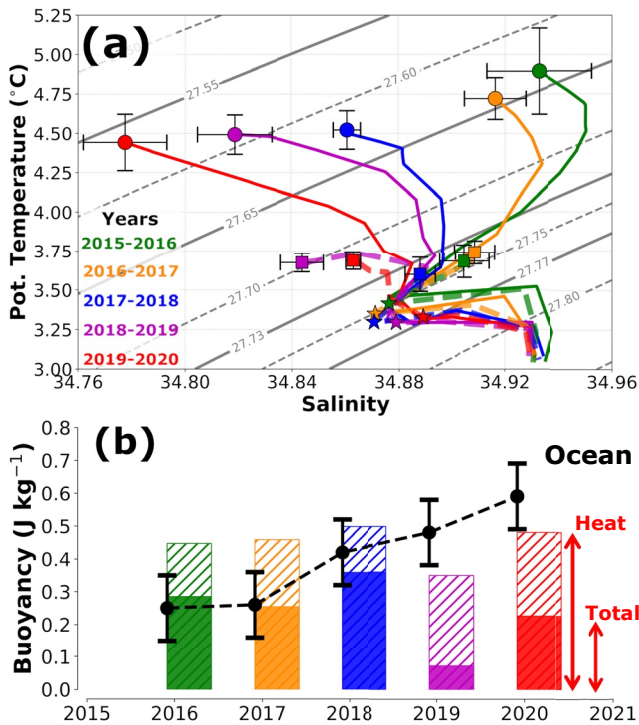


Figure 3. (a) Evolution of the temperature (T) and salinity (S) properties in the interior of the Irminger Sea measured by the FLB mooring. Solid lines are the averaged TS profiles in late fall, while dashed lines represent the same properties in the following late winter. Fall profiles correspond to the month when the ocean had lost the accumulated buoyancy acquired during the spring and summer via B_{flux} (i.e., December). Winter profiles were averaged over the month with the lowest buoyancy content (i.e., April). Circles and squares indicate the respective TS properties near the surface of the fall and winter profiles, while stars are the TS values at approximately 1,000 m depth during both fall and winter. Error bars are the standard errors of the monthly means near the surface. Gray lines are potential density lines in kg m^{-3} . (b) ERA5 reanalysis buoyancy removed from the water column by the atmosphere at the FLB mooring (colored bars) via B_{flux} during wintertime (i.e., December–April). Solid bars are the total buoyancy loss, and hatched bars indicate the buoyancy loss due to heat fluxes. Therefore, difference between solid and hatched bars is the buoyancy gain due to surface freshwater fluxes (e.g., Equation 2). Black circles are the water column buoyancy content in the upper 1,000 m depth of the late fall profiles and its associated standard errors.

the freshening being mainly constrained to water masses lighter than $\sigma_0 \sim 27.73 \text{ kg m}^{-3}$ and impacting the stratification of this upper layer. Consequently, the buoyancy content of the upper 1,000 m approximately doubled between the fall of 2017 ($0.26 \pm 0.10 \text{ J kg}^{-1}$) and the fall of 2019 ($0.59 \pm 0.11 \text{ J kg}^{-1}$; see black dots in Figure 3b). Note that the fall temperatures in the upper ocean did not change significantly from 2016 to 2019.

It is important to mention that the freshening is mainly associated with the gradual erosion of the modified Subpolar Mode Water (SPMW) salinity subsurface maximum in the first $\sim 200 \text{ m}$ (i.e., $27.65 < \sigma_0 < 27.73 \text{ kg m}^{-3}$; e.g., Le Bras et al., 2018; Petit et al., 2021). After the fall of 2018, however, the SPMW salinity signature completely disappears as indicated by the TS properties of the waters lighter than 27.73 kg m^{-3} following almost a straight line (see fall 2019 TS profile). This suggests that waters lighter than 27.73 kg m^{-3} are a mixture of surface waters (salinity $< 34.80 \text{ PSU}$) and waters in the upper ISIW–upper LSW layer.

Water mass formation via wintertime convection is sensitive to the preconditioning of the water column prior to the convection season (i.e., late fall) and the winter atmospheric conditions (e.g., de Jong et al., 2012). Atmospheric-forced deep convection will develop if the atmosphere removes more buoyancy from the ocean during wintertime (i.e., solid bars in Figure 3b) than the ocean’s buoyancy content in the upper 1,000 m (i.e., black dots in Figure 3b).

Consistent with Zunino et al. (2020)’s Argo data south of Greenland, we found that the atmosphere removed enough buoyancy from the water column to homogenize the upper 1,000 m during 2015–2016, 2016–2017, and 2017–2018 winters (Figure 3b), resulting in maximum winter mixed-layer depths between $\sim 1,200\text{--}1,600 \text{ m}$ (e.g., Figure S5 in Supporting Information S1) and outcropping of the $27.74 \pm 0.01 \text{ kg m}^{-3}$ isopycnal. During these winters, the dISIW formed in the central Irminger Sea slightly varied, being the most apparent change the salinity decrease of $\sim 0.02 \text{ PSU}$ near the surface during the 2017–2018 winter (Figure 3a).

In contrast, during the 2018–2019 and 2019–2020 winters, the combined effects of the anomalous stratification due to the GSA arrival and the winter conditions caused the suppression of deep convection (i.e., maximum mixed-layer depths did not exceed $\sim 650 \text{ m}$, Figure S5 in Supporting Information S1). As a result, vertical mixing between surface waters and dISIW–dLSW ceased, forming a low salinity layer cap in the upper $\sim 350 \text{ m}$ that was $0.04\text{--}0.06 \text{ PSU}$ fresher and $\sim 0.03\text{--}0.04 \text{ kg m}^{-3}$ lighter than the water mass formed during the 2015–2016 winter (Figure 3a). Specifically, during the

2018–2019 winter, the mild atmospheric conditions resulted in relatively low buoyancy losses (i.e., magenta solid bar in Figure 3b). However, idealized numerical one-dimensional mixed-layer simulations, or PWP simulations (Price et al., 1986; Våge, 2006; Våge et al., 2008), suggest that deep convection would have halted even under stronger winter atmospheric conditions (Text S5 in Supporting Information S1). In the following year, the accumulated buoyancy losses due to heat fluxes recovered and resembled the earlier years (i.e., 2016–2018). However, because of the buoyancy content increase associated with the GSA, the atmosphere could not remove enough buoyancy from the ocean to promote deep convection (Figure 3b and Figure S5 in Supporting Information S1).

Here, we provided evidence that, as the GSA reached the central Irminger, convection-induced vertical mixing freshened the dISIW–dLSW layers below 1,000 m depth until 2018. From late 2018 forward, the rapid freshening continued to increase local stratification contributing to the shutdown of deep convection in the area for two consecutive winters. Even though convection weakened and winter waters became significantly lighter, wintertime near-surface cooling formed water mass of $\sigma_0 \sim 27.70 \text{ kg m}^{-3}$ (Figure 3a) which constitute the uISIW–

uLSW layer (Le Bras et al., 2020). Note that the lack of vertical mixing and the increase in the surface freshwater fluxes could have locally amplified the GSA signal during 2019, as suggested by Movie S1.

4. Summary and Implications

The present study describes the basin-wide freshening of the Irminger Sea's upper ~200 m between 2015 and 2020 using Argo-based climatology products and hydrographic mooring records. We provide compelling observational evidence that the export of the recent GSA from the Iceland Basin caused a rapid freshening in the Irminger Sea after 2015 (0.02–0.04 PSU year⁻¹), culminating in annually averaged salinities as low as the freshest years of the 1990s and possibly since 1960. The GSA mainly entered the Irminger Sea over the Reykjanes Ridge, impacting the water properties of the Irminger's boundary current. The GSA was then advected around the Irminger Sea within months by the boundary current (~0.1 m s⁻¹) while slowly spreading to the basin's interior. As a result, in the central Irminger, the GSA signal was detected approximately 1 year later and lasted 6 months longer than the signal within the western boundary. Furthermore, the freshening of the central Irminger reduced the salinity of the dISIW produced via deep convection during the 2017–2018 winter and contributed to the halt of the deep convection in the following two winters. The GSA was responsible for doubling the stratification in the upper 1,000 m between 2017 and 2020.

Interestingly, our study could help shed light on the relative importance of different mechanisms that led to the extreme freshening of the Iceland Basin. In both the Iceland and Irminger basins, the ocean layers affected by the GSA after 2015 (Figure 1b) mainly consist of SPMW, which results from the transformation of subtropical-originated water masses in the Iceland Basin (Brambilla & Talley, 2008; Petit et al., 2020). The long term, basin-wide, freshening since 2010 (Figure 1c)—consistent with the NAO-forced low inflow of subtropical waters to the SPNA (Lankhorst & Send, 2020; Tesdal & Haine, 2020)—and the apparent absence of SPMW in the central Irminger (Figure 3a) could indicate that the reduction in the inflow of subtropical water masses to the SPNA played a major role in forming the new GSA. Concurrently, the freshwater redistribution described by Holliday et al. (2020) amplified the ongoing freshening. It is important to mention that to properly quantify the contributions of both mechanisms, a rigorous multiparametric water masses analysis is required (e.g., Fröb et al., 2018). Finally, since late 2017, the NAO phase has reversed, which could herald a possible decade-long salinity recovery in the Irminger Sea from 2020 forward (Desbruyères et al., 2012). In fact, the strong positive salinity trends in the eastern North Atlantic (Figure 1a) seem to support this idea.

To conclude, recent studies place the Irminger Sea as a crucial formation region of water masses that constitute the deep limb of the AMOC. Both atmospheric-driven cooling within the boundary current system and deep convection in the interior play an essential role in the overturning of the SPNA (Le Bras et al., 2020). Differently to the Labrador Sea where deep convection occurs more regularly (e.g., Yashayev & Loder, 2016), deep convection in the Irminger Sea is intermittent and sensitive to the right combinations of water column preconditioning and atmospheric forcing (Zunino et al., 2020). Here, we showed indirect evidence that zonal flows over the Reykjanes Ridge help control the water properties in the Irminger Sea basin-wide (Section 3.2). To accurately predict the hydrographic properties of the AMOC's lower limb and the amount of heat and carbon exported out of the SPNA to lower latitudes, climate models will likely have to accurately predict salt and heat fluxes over the narrow fractures of the Reykjanes Ridge.

Data Availability Statement

All data used in this study are available online, and it can be accessed as follows: OSNAP mooring data (<https://www.o-snap.org/observations/data/>) under “US East Cape Farewell Slope Array” and “US Eastern Mid-Atlantic-Ridge Array”; OOI (<https://ooinet.oceanobservatories.org/platformnav?id=R0kwM0ZMTUI=&array=R2x-vYmFsIElybWluZ2VyIFNlYQ==&lat=NTkuNzE4Mg==&lng=LTM5LjM1MzY=>, accessed on 13 November 2020); RG-climatology (https://sio-argo.ucsd.edu/RG_Climatology.html, accessed on 20 October 2020); EN4-climatology (<https://hadleyserver.metoffice.gov.uk/en4/download-en4-2-1.html>, accessed on 5 May 2021); ERA5 reanalysis (<https://doi.org/10.24381/cds.adbb2d47>, accessed on 2 July 2021); quality-controlled individual Argo profiles (<https://doi.org/10.17882/42182>, accessed on 25 October 2020); GLORYS12 ocean reanalysis (<https://doi.org/10.48670/moi-00021>, accessed on 17 February 2022); ARMOR3D hydrographic climatology (<https://doi.org/10.48670/moi-00052>, accessed on 18 February 2022); General Bathymetric Chart of the Oceans

(https://www.gebco.net/data_and_products/gridded_bathymetry_data/, accessed on 9 April 2021); Ssalto/Duacs altimeter products (<https://doi.org/10.48670/moi-00148>, accessed on 3 November 2020); Global Drifters Program (https://www.aoml.noaa.gov/phod/gdp/hourly_data.php accessed on 18 January 2021).

Acknowledgments

We gratefully acknowledge the US National Science Foundation for funding this work under grants OCE-1258823, OCE-1756272, OCE-1948335, and OCE-2038481. The calibrated and quality-controlled RR mooring data used in this study were generously provided by Dr Bill Johns from the University of Miami. We also acknowledge the two anonymous reviewers for their insightful comments. Finally, we thank the many scientists and mariners involved in the OSNAP and OOI projects who went to sea to collect the observational data used in this work.

References

- Argo. (2020). Argo float data and metadata from Global Data Assembly Centre (Argo GDAC). [Data Set]. SEANOE. <https://doi.org/10.17882/42182>
- Belkin, I. M. (2004). Propagation of the “Great Salinity Anomaly” of the 1990s around the northern North Atlantic. *Geophysical Research Letters*, *31*, L08306. <https://doi.org/10.1029/2003GL019334>
- Belkin, I. M., Levitus, S., Antonov, J., & Malmberg, S. (1998). “Great Salinity Anomalies” in the North Atlantic. *Progress in Oceanography*, *41*(1), 1–68. [https://doi.org/10.1016/S0079-6611\(98\)00015-9](https://doi.org/10.1016/S0079-6611(98)00015-9)
- Biló, T. C., & Johns, W. E. (2019). Interior pathways of Labrador Sea Water in the North Atlantic from the Argo perspective. *Geophysical Research Letters*, *46*, 3340–3348. <https://doi.org/10.1029/2018GL081439>
- Brambilla, E., & Talley, L. D. (2008). Subpolar Mode Water in the northeastern Atlantic: 1. Averaged properties and mean circulation. *Journal of Geophysical Research*, *113*, C04025. <https://doi.org/10.1029/2006JC004062>
- Curry, R., & Mauritzen, C. (2005). Dilution of the northern North Atlantic Ocean in recent decades. *Science*, *308*(5729), 1772–1774. <https://doi.org/10.1126/science.1109477>
- Dee, D. P., Uppala, S. M., Simmons, A. J., Berrisford, P., Poli, P., Kobayashi, S., et al. (2011). The ERA-Interim reanalysis: Configuration and performance of the data assimilation system. *Quarterly Journal of the Royal Meteorological Society*, *137*(656), 553–597. <https://doi.org/10.1002/qj.828>
- de Jong, F. M., Oltmanns, M., Karstensen, J., & de Steur, L. (2018). Deep convection in the Irminger Sea observed with a dense mooring array. *Oceanography*, *31*(1), 50–59. <https://doi.org/10.5670/oceanog.2018.109>
- de Jong, F. M., Steur, L., Fried, N., Bol, R., & Kritsotakis, S. (2020). Year-round measurements of the Irminger current: Variability of a two-core current system observed in 2014–2016. *Journal of Geophysical Research: Oceans*, *125*, e2020JC016193. <https://doi.org/10.1029/2020JC016193>
- de Jong, F. M., van Aken, H. M., Våge, K., & Pickart, R. S. (2012). Convective mixing in the central Irminger Sea: 2002–2010. *Deep Sea Research Part I: Oceanographic Research Papers*, *63*, 36–51. <https://doi.org/10.1016/j.dsr.2012.01.003>
- Desbryères, D., Chafik, L., & Maze, G. (2021). A shift in the ocean circulation has warmed the Subpolar North Atlantic Ocean since 2016. *Communications Earth & Environment*, *2*(1), 48. <https://doi.org/10.1038/s43247-021-00120-y>
- Dickson, R. R., Meincke, J., Malmberg, S., & Lee, A. J. (1988). The “Great Salinity Anomaly” in the northern North Atlantic 1968–1982. *Progress in Oceanography*, *20*(2), 103–151. [https://doi.org/10.1016/0079-6611\(88\)90049-3](https://doi.org/10.1016/0079-6611(88)90049-3)
- Eliot, S., Lumpkin, R., Perez, R. C., Lilly, J. M., Early, J. J., & Sykulski, A. M. (2016). A global surface drifter data set at hourly resolution. *Journal of Geophysical Research: Oceans*, *121*, 2937–2966. <https://doi.org/10.1002/2016JC011716>
- Emery, W. J., & Thomson, R. E. (2001). *Data analysis methods in physical oceanography*. Elsevier.
- Fan, X., Send, U., Testor, P., Karstensen, J., & Lherminier, P. (2013). Observations of Irminger Sea anticyclonic eddies. *Journal of Physical Oceanography*, *43*(4), 805–823. <https://doi.org/10.1175/JPO-D-11-0155.1>
- Fröb, F., Olsen, A., Pérez, F. F., García-Ibáñez, M. I., Jeansson, E., Omar, A., & Lauvset, S. K. (2018). Inorganic carbon and water masses in the Irminger Sea since 1991. *Biogeosciences*, *15*(1), 51–72. <https://doi.org/10.5194/bg-15-51-2018>
- Fröb, F., Olsen, A., Våge, K., Moore, G. W. K., Yashayaev, I., Jeansson, E., & Rajasakaren, B. (2016). Irminger Sea deep convection injects oxygen and anthropogenic carbon to the ocean interior. *Nature Communications*, *7*(1), 13244. <https://doi.org/10.1038/ncomms13244>
- Gill, A. E. (1982). *Atmosphere–ocean dynamics*. San Diego, CA: Academic Press.
- Good, S. A., Martin, M. J., & Rayner, N. A. (2013). EN4: Quality controlled ocean temperature and salinity profiles and monthly objective analyses with uncertainty estimates. *Journal of Geophysical Research: Oceans*, *118*, 6704–6716. <https://doi.org/10.1002/2013JC009067>
- Gouretski, V., & Reseghetti, F. (2010). On depth and temperature biases in bathythermograph data: Development of a new correction scheme based on analysis of a global ocean database. *Deep Sea Research Part I: Oceanographic Research Papers*, *57*(6), 812–833. <https://doi.org/10.1016/j.dsr.2010.03.011>
- Guinehut, S., Dhomp, A., Larnicol, G., & Le Traon, P. (2012). High resolution 3-D temperature and salinity fields derived from in situ and satellite observations. *Ocean Science*, *8*(5), 845–857. <https://doi.org/10.5194/os-8-845-2012>
- Häkkinen, S., & Rhines, P. (2004). Decline of Subpolar North Atlantic circulation during the 1990s. *Science*, *304*(5670), 555–559. <https://doi.org/10.1126/science.1094917>
- Hátún, H., Sandø, A. B., Drange, H., Hansen, B., & Valdimarsson, H. (2005). Influence of the Atlantic subpolar gyre on the thermohaline circulation. *Science*, *309*(5742), 1841–1844. <https://doi.org/10.1126/science.1114777>
- Holliday, P. N., Bacon, S., Allen, J., & McDonagh, E. (2009). Circulation and transport in the western boundary currents at Cape Farewell, Greenland. *Journal of Physical Oceanography*, *39*(8), 1854–1870. <https://doi.org/10.1175/2009JPO4160.1>
- Holliday, P. N., Bersch, M., Berx, B., Chafik, L., Cunningham, S., Florindo-López, C., et al. (2020). Ocean circulation causes the largest freshening event for 120 years in eastern Subpolar North Atlantic. *Nature Communications*, *11*(1), 585. <https://doi.org/10.1038/s41467-020-14474-y>
- Holliday, P. N., Meyer, A., Bacon, S., Alderson, S. G., & de Cuevas, B. (2007). Retroflexion of part of the east Greenland current at Cape Farewell. *Geophysical Research Letters*, *34*, L07609. <https://doi.org/10.1029/2006GL029085>
- Holte, J., & Straneo, F. (2017). Seasonal overturning of the Labrador Sea as observed by Argo floats. *Journal of Physical Oceanography*, *47*(10), 2531–2543. <https://doi.org/10.1175/JPO-D-17-0051.1>
- Hopkins, J. E., Holliday, P. N., Rayner, D., Houpert, L., Le Bras, I. A. A., Straneo, F., et al. (2019). Transport variability of the Irminger Sea deep western boundary current from a mooring array. *Journal of Geophysical Research: Oceans*, *124*, 3246–3278. <https://doi.org/10.1029/2018JC014730>
- Jean-Michel, L., Greiner, E., Bourdallé-Badie, R., Gilles, G., Angélique, M., Drévilion, M., et al. (2021). The Copernicus global 1/12° oceanic and sea ice GLORYS12 reanalysis. *Frontiers of Earth Science*, *9*, 1–27. <https://doi.org/10.3389/feart.2021.698876>
- Koman, G., Johns, W. E., & Houk, A. (2020). Transport and evolution of the east Reykjanes Ridge current. *Journal of Geophysical Research: Oceans*, *125*, e2020JC016377. <https://doi.org/10.1029/2020JC016377>
- Lankhorst, M., & Send, U. (2020). Uncertainty of North Atlantic current observations from altimetry, floats, moorings, and XBT. *Progress in Oceanography*, *187*, 102402. <https://doi.org/10.1016/j.pocan.2020.102402>

- Lazier, J. R. N. (1980). Oceanographic conditions at Ocean Weather Ship *Bravo*, 1964–1974. *Atmosphere-Ocean*, 18(3), 227–238. <https://doi.org/10.1080/07055900.1980.9649089>
- Le Bras, I. A. A.-A., Straneo, F., Holte, J., de Jong, F. M., & Holliday, P. N. (2018). Seasonality of freshwater in the east Greenland current system from 2014 to 2016. *Journal of Geophysical Research: Oceans*, 123, 8828–8848. <https://doi.org/10.1029/2018JC014511>
- Le Bras, I. A. A.-A., Straneo, F., Holte, J., de Jong, F. M., & Holliday, P. N. (2020). Rapid export of waters formed by convection near the Irminger Sea's western boundary. *Geophysical Research Letters*, 47, e2019GL085989. <https://doi.org/10.1029/2019GL085989>
- Lozier, S. M. (2010). Deconstructing the conveyor belt. *Science*, 328(5985), 1507–1511. <https://doi.org/10.1126/science.1189250>
- Lozier, S. M. (2012). Overturning in the North Atlantic. *Annual Review of Marine Science*, 4(1), 291–315. <https://doi.org/10.1146/annurev-marine-120710-100740>
- Lozier, S. M., Li, F., Bacon, S., Bahr, F., Bower, A. S., Cunningham, S. A., et al. (2019). A sea change in our view of Overturning in the Subpolar North Atlantic. *Science*, 363, 516–521. <https://doi.org/10.1126/science.aau6592>
- McDougall, T. J., & Barker, P. M. (2011). *Getting started with TEOS-10 and the Gibbs Seawater (GSW) Oceanographic Toolbox* (Tech. Rep. SCOR/IAPSO WG127). Retrieved from <http://www.teos-10.org/software.htm>
- Miron, P., Beron-Vera, F. J., Olascoaga, J. M., Sheinbaum, J., Pérez-Brunius, P., & Froyland, G. (2017). Lagrangian dynamical geography of the Gulf of Mexico. *Scientific Reports*, 7(1), 7021. <https://doi.org/10.1038/s41598-017-07177-w>
- Petit, T., Lozier, S. M., Josey, S. A., & Cunningham, S. A. (2020). Atlantic deep water formation occurs primarily in the Iceland basin and Irminger Sea by local buoyancy forcing. *Geophysical Research Letters*, 47, e2020GL091028. <https://doi.org/10.1029/2020GL091028>
- Petit, T., Lozier, S. M., Josey, S. A., & Cunningham, S. A. (2021). Role of air–sea fluxes and ocean surface density in the production of deep waters in the eastern subpolar gyre of the North Atlantic. *Ocean Science*, 17(5), 1353–1365. <https://doi.org/10.5194/os-17-1353-2021>
- Petit, T., Mercier, H., & Thierry, V. (2018). First direct estimates of volume and water mass transports across the Reykjanes Ridge. *Journal of Geophysical Research: Oceans*, 123, 6703–6719. <https://doi.org/10.1029/2018JC013999>
- Petit, T., Mercier, H., & Thierry, V. (2019). New insight into the formation and evolution of the east Reykjanes Ridge current and Irminger current. *Journal of Geophysical Research: Oceans*, 124, 9171–9189. <https://doi.org/10.1029/2019JC015546>
- Pickart, R. S., Straneo, F., & Moore, G. W. K. (2003). Is Labrador Sea Water formed in the Irminger basin? *Deep Sea Research Part I: Oceanographic Research Papers*, 50(1), 23–52. [https://doi.org/10.1016/S0967-0637\(02\)00134-6](https://doi.org/10.1016/S0967-0637(02)00134-6)
- Piron, A., Thierry, V., Mercier, H., & Caniaux, G. (2016). Argo float observations of basin-scale deep convection in the Irminger Sea during winter 2011–2012. *Deep Sea Research Part I: Oceanographic Research Papers*, 109, 76–90. <https://doi.org/10.1016/j.dsr.2015.12.012>
- Price, J. F., Weller, R. A., & Pinkel, R. (1986). Diurnal cycling: Observations and models of the upper ocean response to diurnal heating, cooling, and wind mixing. *Journal of Geophysical Research*, 91(C7), 8411–8427. <https://doi.org/10.1029/JC091iC07p08411>
- Roemmich, D., & Gilson, J. (2009). The 2004–2008 mean and annual cycle of temperature, salinity, and steric height in the global ocean from the Argo program. *Progress in Oceanography*, 82(2), 81–100. <https://doi.org/10.1016/j.pocean.2009.03.004>
- Schmidt, S., & Send, U. (2007). Origin and composition of seasonal Labrador Sea freshwater. *Journal of Physical Oceanography*, 37(6), 1445–1454. <https://doi.org/10.1175/JPO3065.1>
- Tesdal, J.-E., Abernathey, R. P., Goes, J. I., Gordon, A. L., & Haine, T. W. N. (2018). Salinity trends within the upper layers of the Subpolar North Atlantic. *Journal of Climate*, 31(7), 2675–2698. <https://doi.org/10.1175/JCLI-D-17-0532.1>
- Tesdal, J.-E., & Haine, T. W. N. (2020). Dominant terms in the freshwater and heat budgets of the Subpolar North Atlantic Ocean and Nordic Seas from 1992 to 2015. *Journal of Geophysical Research: Oceans*, 125, e2020JC016435. <https://doi.org/10.1029/2020JC016435>
- Våge, K. (2006). *Winter mixed-layer development in the central Irminger Sea: The effect of strong, intermittent wind events* (Master's thesis). Massachusetts Institute of Technology and Woods Hole Oceanographic Institute.
- Våge, K., Pickart, R. S., Moore, G. W. K., & Ribergaard, M. H. (2008). Winter mixed layer development in the central Irminger Sea: The effect of strong, intermittent wind events. *Journal of Physical Oceanography*, 38(3), 541–565. <https://doi.org/10.1175/2007JPO3678.1>
- Våge, K., Pickart, R. S., Sarafanov, A., Knutsen, O., Mercier, H., Lherminier, P., et al. (2011). The Irminger gyre: Circulation, convection, and interannual variability. *Deep Sea Research Part I: Oceanographic Research Papers*, 58(5), 590–614. <https://doi.org/10.1016/j.dsr.2011.03.001>
- Våge, K., Pickart, R. S., Thierry, V., Reverdin, G., Lee, C. M., Petrie, B., et al. (2009). Surprising return of deep convection to the Subpolar North Atlantic Ocean in winter 2007–2008. *Nature Geoscience*, 2(1), 67–72. <https://doi.org/10.1038/ngeo382>
- Yashayaev, I., & Loder, J. M. (2016). Recurrent replenishment of Labrador Sea Water and associated decadal-scale variability. *Journal of Geophysical Research: Oceans*, 121, 8095–8114. <https://doi.org/10.1002/2016JC012046>
- Zunino, P., Mercier, H., & Thierry, V. (2020). Why did deep convection persist over four consecutive winters (2015–2018) southeast of Cape Farewell? *Ocean Science*, 16(1), 99–113. <https://doi.org/10.5194/os-16-99-2020>